Raman scattering from a partly interrupted network glass former

1990 J. Phys.: Condens. Matter 2 2303

(http://iopscience.iop.org/0953-8984/2/9/019)

J. Phys.: Condens. Matter **2** (1990) 2303–2330. Printed in the UK

Raman scattering from a partly interrupted network glass former

J Sukmanowski†, I Petscherizin‡, M Soltwisch† and D Quitmann†

† Institut für Atom- und Festkörperphysik, Freie Universität Berlin, Arnimallee 14, D1000 Berlin 33, Federal Republic of Germany

‡ Chemical Institute, University of Leningrad, USSR

Received 21 March 1989, in final form 19 October 1989

Abstract. We have studied the Raman spectra of a network glass former that derives from GeS_2 by interrupting the sulphur bridges by two halogens, concentrating on $GeSBr_2$ where on average two of the four bridges per $GeS_{4/2}$ tetrahedron are interrupted. The temperature range was 520–230 K (glass transition temperature $T_g = 250$ K). At a resolution of 2 cm^{-1}, a rich structure develops instead of the very broad lines of GeS_2 glass. We concentrate on the lines that derive from the tetrahedral A_1 (breathing) mode. In order to analyse them, we use a program for eigenfrequencies and eigenvectors neglecting symmetries (NORCOR of D Christen). Electro-optical parameters are estimated from the bond polarisability model. We consider quasi-molecular subunits of one, two or three tetrahedra with S or Br substituents. Then the fine structure of the Raman spectra can be understood as due to intermediate-range order, viz. coupling of neighbouring tetrahedra, probability of occurrence of various possible subunits and their geometrical configuration; about 100 subunits are included. A very satisfactory simulation of the Raman spectrum for the said modes is achieved. Edge-connected bitetrahedra and chair-shaped rings are essentially absent. Force constants show only minor changes.

1. Introduction

Glasses form from essentially all types of atomic or molecular units (covalently bonding atoms, covalent and ionic compounds, metals, etc). They are characterised by the conflicting situations of a local (nearest-neighbour) order virtually identical to crystals, but no long-range order at all, rather isotropy and homogeneity. The intermediate-range order (second, third neighbours) has a broader range of variation and allows one to reconcile the apparently conflicting short- and long-range orders. It is generally assumed that the order in the glass state is a smooth, probably identical continuation of structural order as it exists in the liquid equilibrium state. According to the most recent group of studies (Leutheusser 1984, Bengtzelius *et al* 1984, Bosse and Thakur 1988), the glass transition is a characteristic, prolonged kinematic slowing down, correlated with very small structural changes. In these studies, model hard-sphere systems have been treated. The majority of real glasses are network glass formers, and are a long-standing subject because of their technical importance (SiO_2, a-Si, fibres) and their challenge to our understanding of systems where limited disorder is essential (Elliott 1987a, b, Lannin 1987).

0953-8984/90/092303 + 28 $03.50

GeS_2 is a well studied system (Rowland *et al* 1972, Lucovsky *et al* 1974a, b, Lucovsky 1987, Kawamoto and Kawashima 1982, Tenhover *et al* 1985, Drahokoupil *et al* 1986, Arai 1983), which forms a glass of $GeS_{4/2}$ tetrahedral units interconnected via S. The tetrahedra constitute identical basic units for a network *if* no bonds between like atoms and no double bonds exist; although that requirement may not be strictly satisfied (Phillips 1981), the network will be very extended.

While there exist many models for interconnected tetrahedra, it is notoriously difficult to extract from experimental data structural information beyond the nearest-neighbour shell, i.e. about intermediate-range order. For recent discussions of intermediate-range order in liquid and amorphous chalcogenides, see Elliott (1987a, b), Lannin (1987), Lucovsky (1987), Price *et al* (1987) and Cervinka (1987). One of the major means of experimental access to structure is Raman scattering, but the Raman spectra of glasses usually consist of a few rather broad features. Analysis of the spectra considers the Ge-centred tetrahedra as the quasi-molecular building unit and concentrates on the breathing mode (A_1 mode, positioned at $\nu_1 = 396\ cm^{-1}$ in the tetrahedral $GeCl_4$ molecule), partly because in glasses it remains the most strongly Raman-active mode. It is used, for example, in the comparison of α- and β-phase crystalline GeS_2 with GeS_2 glass (Kawamoto and Kawashima 1982). In the $GeS_{4/2}$ glass, the featureless broadening of the breathing mode into the 340 cm^{-1} peak offers, however, no clue for a more detailed study of intermediate-range order, or of variations in connectivity (edge sharing versus corner sharing) or even of the causes of broadening, which may be strains in the Ge–S–Ge bond angle or in the Ge–S bond distance. Yet the tetrahedral breathing mode has served as the most important source of information in many studies of tetrahedral network glasses (Kawamoto and Kawashima 1982, Tenhover *et al* 1985, Lucovsky *et al* 1974a, b).

Here we study the effects of cutting the network connections by inserting halogen X, $GeS_{4/2} \rightarrow GeS_{2-N/2}X_N$, and of melting on the modes deriving from the tetrahedral A_1 mode. Such cutting relieves the causes of broadening. The situation intermediate between independent molecules and a true glass makes the system a testing ground for methods to study intermediate-range order. One price to be paid is that the substitution creates tetrahedra with different numbers of S and halogen corners, introducing new splittings. Fortunately, these splittings are *larger* than intermediate-range order effects. One arrives at a Raman spectrum rather rich in lines, where the half-widths of these lines (about 3–5 cm^{-1}) are now an order of magnitude smaller than that of the GeS_2 glass tetrahedral breathing mode (FWHM 50 cm^{-1}). The narrow width results from relieving the strains and from decoupling. Another uncertainty introduced by partly saturating Ge by halogen is the occurrence of true molecular species, i.e. with no bonds to the network, like $GeBr_4$, dimers, trimers or rings, etc.

Figure 1 gives examples from the spectra for the $GeSBr_2$ system. When the melt is cooled down towards the glass transition temperature, we find surprisingly small changes in gross and fine structure—position, width, intensity and depolarisation—although the coupling between the tetrahedral subunits must become stronger.

The new information apparently concealed in these spectra, as well as in the rich literature data on Raman spectroscopy of chalcogenide glass formers, made it a challenge to try and pave the way for an interpretation of the Raman spectra of disordered network systems, especially in terms of intermediate-range order. We present here such an attempt, which is based on the model of quasi-molecular subunits (Lucovsky and Martin 1972), as a mathematically tractable starting point, and on statistical and stereochemical assumptions for the probabilities of subunits and of their interconnections; included is

the use of electro-optical parameters, which are good approximations for the modes and the systems considered.

The experimental results are presented in § 3. The aim of the discussion is then to simulate the spectrum of the $GeSBr_2$ system, using as much as possible 'reliable' input data. This simulation starts by calculating eigenfrequencies and eigenvectors for (molecule-like) subunits. A suitable computer program, NORCOR, has been kindly put at our disposal by Dr D Christen (1978). These calculations are described in § 4.2, results being summarised in § 4.2.3. The calculation of intensities for subunits is described in § 4.3. Besides the procedure and the bond polarisability model (§ 4.3.1), it includes a formulation of the scheme used here to build up the relevant subunits (§§ 4.3.4 and 4.3.5). Results, including the final simulation spectrum, will be presented in § 4.3.6. We conclude that the systems studied can in fact be treated along these lines, and that the analysis of the Raman spectra is possible on at least a semiquantitative level (§ 5).

Raman studies of $Ge_xS_yBr_z$ have also been done recently, though with low resolution, by Koudelka *et al* (1987). This work and the present one complement each other in the respect that Koudelka *et al* have mainly studied the concentration dependence of the intensities of the broad lines that they have registered upon variation of x in $(GeS_2)_{1-x}(GeBr_4)_x$, $0 \leq x \leq 0.81$. The present work considers reasonably well decoupled systems (mostly $x = 0.5$), their temperature dependence, and concentrates on the fine structure seen. Additional work on Brillouin scattering from $GeSBr_2$ is in progress (Loheider *et al* 1990).

2. Experimental details

2.1. Sample preparation

Sample materials GeS_xBr_y ($x/y = 1/2$, $3/2$) were prepared from the pure elements (Ge 99.9999%, S 99.99%, Br 99.9%) essentially in two steps. A sealed quartz vessel contained aliquots of elemental Ge and S on the bottom, and Br_2 in an additional small open cup. Upon mild heating ($T < 150$ °C), a red substance appears (presumably $S + Br_2 \rightarrow SBr_2$). When heating further (150–250 °C in 4–6 h), the exothermic Ge–S reaction starts. After keeping the vessel at 300 °C for about 12 h, a low-viscosity colourless liquid has formed, with black pieces in and on top of it (presumably GeS). The sample is then heated further (Ge–Br reactions), kept at 500–600 °C for 12 h, cooled to 100 °C and later to room temperature. It is now a clear, highly viscous fluid with very few black grainlets; these disappear almost completely after renewed heating to 600 °C. In the preparation, amounts of 10–20 g were used. After the synthesis, the samples were transferred under N_2 to cylindrical or thin plane quartz containers, which were evacuated and sealed.

GeS_2 was commercial (Merck) and was quenched in a sealed quartz vessel from 1000 °C or from 600 °C. Reference samples $GeBr_4$, $GeCl_4$ and GeI_4 were commercial (Merck); $GeBr_4$ and $GeCl_4$ were mixed under an Ar atmosphere.

2.2. Raman scattering experiments

The set-up consists basically of an ion laser (4 W Ar or 1 W Kr, Spectra 165, multimode) and a 1 m double monochromator (Jobin Yvon U1000, 1800 lines/mm) with photon counting (cooled photomultiplier ITFW 130, dark count rate $1\ s^{-1}$). A fast counter

is followed by data accumulation in an experiment-assigned computer (LSI 11/23). Resolution of the monochromator was set at values between 0.7 and 2 cm^{-1}. Unless otherwise stated, the 5145 Å line was used, Spectra were typically taken using 512 channels, 1 cm^{-1} each, with a single sweep from low- to high-frequency displacements on the anti-Stokes side, measurement times being 1 to 6 s per channel, 50–250 mW incident power. Laser intensity was stable within 5% during any single sweep.

The samples were contained in sealed cylindrical quartz ampoules of 5–10 mm ID; one of them was in a 1 cm^2, 0.2 mm wide plane–parallel quartz cuvette. We have usually measured in a 90° arrangement, with a slightly focused, horizontally incoming beam ($f = 10$ cm) and 1:1 imaging onto the entrance slit by two $f = 10$ cm lenses. For polarisation analysis, use was made of the fact that the incoming beam was vertically (V) polarised, and could be turned to horizontal (H) by a $\lambda/2$ plate, and an analysing Nicol prism was inserted (V or H) between the two lenses of the outgoing light path. Usually, after each VV spectrum a depolarised spectrum (HV) was taken for the same temperature. While scanning the spectrometer over the elastic line, the incident beam was almost completely blocked so that only a reduced elastic signal remained as a check; no 'after effect' following the switch-off was observed. The scale of the Raman spectra is accurate to about 1 cm^{-1}.

The scattering intensity was checked beyond 500 cm^{-1}. No scattering comparable at all to the region $\nu \leqslant 500$ cm^{-1} was seen. Background count rate (about 10^2 s^{-1}) was small except when taking depolarised spectra.

For measurements at elevated temperature, the samples were mounted in a furnace, similar to the one described in Soltwisch *et al* (1987). For lower temperatures, an evacuated cryostat was used. The sample was suspended below a liquid-nitrogen-cooled copper block, in a double-walled glass cryostat. The change of polarisation in the quartz (or glass) was checked and found to be small. NiCr thermocouples attached to the sample were used for temperature measurement.

3. Data and phenomenological interpretation

3.1. Spectra

About 100 spectra were taken for the various compositions, temperatures and laser lines (see figures 1–3). For the figures, we reduce the registered spectra I_{reg} to obtain I_{exp} as

$$I_{exp}(\nu) = \nu(\nu_i - \nu)^{-4}(1 - e^{-h\nu/k_B T})I_{reg}(\nu) \tag{1}$$

where ν_i is the frequency of the incident (laser) photons and ν is the frequency relative to the laser frequency. The background was usually not subtracted because it is small, both at $\nu \geqslant 510$ cm^{-1} and between the elastic line and the 'boson peak', i.e. at 5–10 cm^{-1}. In the figures, experimental spectra are not normalised to each other.

The glass temperatures are known either from sound velocity measurements ($GeSBr_2$ (Loheider *et al* 1990)) or from the literature (GeS_2 (Kawamoto and Tsuchihashi 1971)). Upon cooling the $GeSBr_2$ samples, one observes the characteristic huge increase in viscosity, eventually with a cracking of the sample into many pieces separated by irregular cracks, each piece still being clear and homogeneous; a Raman spectrum was then taken after selecting one of the pieces by optical adjustment.

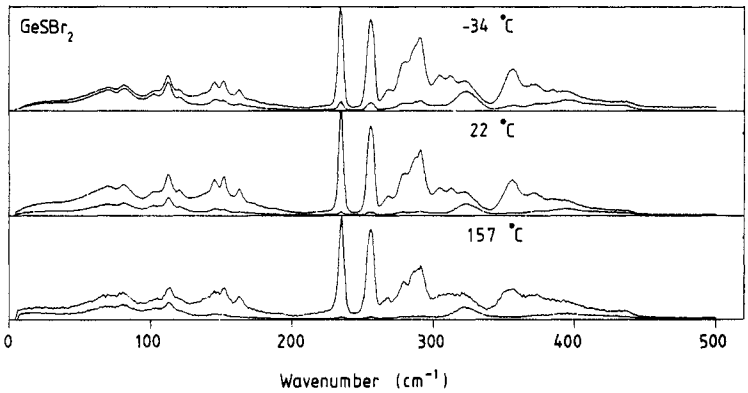

Figure 1. Raman spectra of the $GeSBr_2$ system as a function of temperature taken with $\lambda_0 =$ 514.5 nm. The temperature −34 °C is close to the glass transition, while at 157 °C the structural relaxation time is about 10^{-11} s (Loheider *et al* 1990). VV and HV spectra are displayed. Spectra of $GeSBr_2$ taken at other λ_0 values appear in figures 2 and 3.

3.1.1. $GeSBr_2$. This is the composition most intensively studied in the present work. Figures 1, 2 and 3 show some spectra. (For the infrared (IR) spectrum, see Sukmanowski (1990).) Generally no differences exceeding reproducibility and statistical scatter were observed between the various samples, as a function of laser power or laser frequency, or upon change of other experimental conditions.

A simple decomposition into Lorentzians plus a sloping background $B(\nu)$ was applied to groups of up to four lines in the region 250–350 cm^{-1}. Resulting positions, linewidths and relative intensities are presented in table 1.

The group of lines at 230–310 cm^{-1} is strongly polarised, and in the group extending from 340 to 450 cm^{-1} polarisation is also strong at the lower end (340–380 cm^{-1}). In the figures we include the depolarised spectra. The broad structure at 325 cm^{-1} is seen to be depolarised; it derives from the higher F_2 mode of the tetrahedra. The line at 236 cm^{-1} is the $GeBr_4$ breathing mode (see figure 8(*b*)). The polarised lines in the range 200–400 cm^{-1} are the modes deriving from the breathing mode of tetrahedral subunits $GeS_{2-N/2}X_N$, X = halogen, $N = 4, 3, 2, 1, 0$. This assignment is in accord with earlier work on this or similar systems (Lucovsky *et al* 1974a, b, Boolchand *et al* 1986, Tenhover *et al* 1985, Koudelka *et al* 1987, Kawamoto and Kawashima 1982). From the model calculations for the $GeSBr_2$ system, to be discussed in § 4, and from the mixed $GeCl_4$/$GeBr_4$ system (figure 8(*b*)) it follows that the breathing modes for the $N = 4, 3, 2, 1, 0$ tetrahedra in the Ge–S–Br system are to be expected at about 235, 255, 285, 305 and 395 cm^{-1}, respectively. In the following, we shall often refer loosely to these 'lines' or 'groups' by their N, and to the tetrahedral breathing-mode-derived modes as the TBD modes. The glass temperature of the $GeSBr_2$ system is $T_g = -30$ °C (Loheider *et al* 1990).

3.1.2. GeS_2 and $GeS_{3/2}Br$. GeS_2 is here the starting point as the unperturbed, i.e. maximum connected, network glass former; figure 2 shows its Raman spectrum. A sample with composition $GeS_{3/2}Br$ (figure 2) shows a broad structure at 320–450 cm^{-1}. Also, furthermore, the $GeBr_4$ and $GeS_{1/2}Br_3$ lines ($N = 4, 3$) may be seen, and a clear increase in intensity in the group of the $GeS_{2/2}Br_2$, $GeS_{3/2}Br$ tetrahedra ($N = 2, 1$; 260–310 cm^{-1}), apparently with no shifts in the positions of the lines at 267, 305 and 325 cm^{-1}.

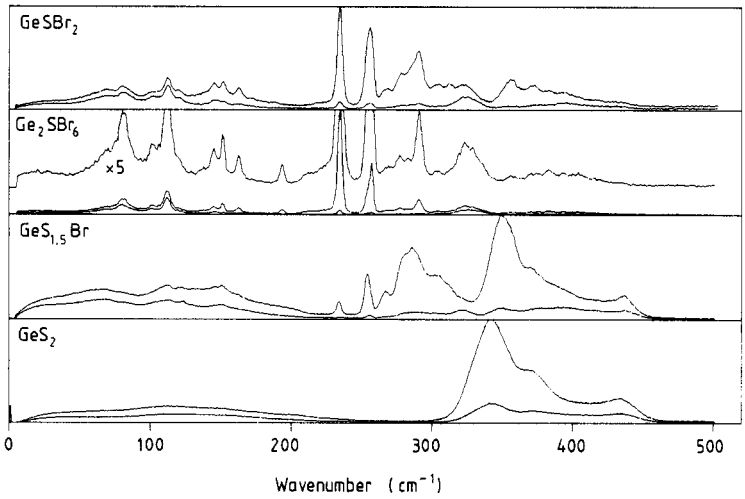

Figure 2. Spectra of the GeS_xBr_y system at different concentrations x and y. Here, $\lambda_0 = 674$ nm, $T = 25$ °C. The GeS_2 glass was quenched from 1000 °C; the other systems are liquid.

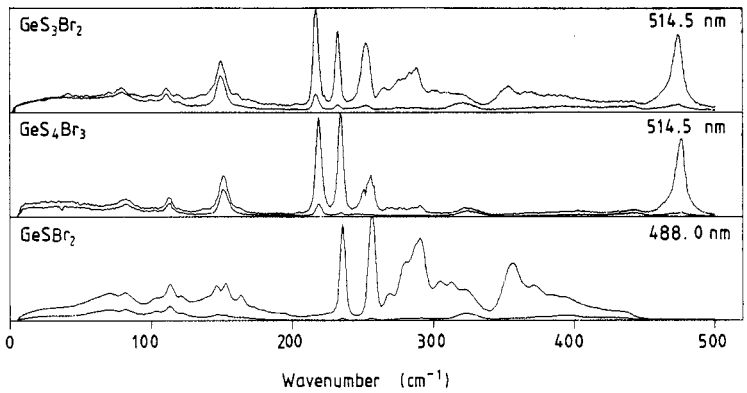

Figure 3. Spectra of liquid S-rich Ge–S–Br systems, and of $GeSBr_2$ taken with $\lambda_0 = 488$ nm. Here $T = 22$ °C.

3.1.3. GeS_3Br_2, GeS_4Br_3 and Ge_2SBr_6. The sulphur-rich light-yellow sample GeS_3Br_2 yields a Raman spectrum (figure 3) characterised by additional strong lines at 150, 210 and 480 cm^{-1}; they also occur in GeS_4Br_3 (see figure 3). These lines prove the presence of molecular sulphur. Apart from that, the spectrum is the same as for $GeSBr_2$; in particular there is no intensity increase in the spectral region of sulphur-rich tetrahedra ($N = 2, 1$; 280–310 cm^{-1}), relative to the Br-rich tetrahedra ($N = 4, 3$).

The colourless sample with composition Ge_2SBr_6 was chosen to increase the probability of a true molecular species of this composition (Krebs 1983) composed of two tetrahedra, coupled via one bridging S. In the Raman spectrum (figure 2), the corresponding line at 256 cm^{-1} is indeed comparatively strong. Unfortunately, $GeBr_4$ had

also been produced. Correspondingly, there is some remnant of S-richer tetrahedra $GeS_{2/2}Br_2$ (280–300 cm^{-1}); but the $GeS_{3/2}Br$ and $GeS_{4/2}$ groups are essentially absent.

3.2. Reactions

On the level of single Ge tetrahedra, the substitution (i.e. the probability of occurrence of N in $GeS_{4-N/2}Br_N$) may be anticipated to shift, depending on the method of preparation, temperature, or local parameters like strain, steric effects, etc. Net reactions would change the intensities of lines or groups of lines, perhaps also change the linewidths (in particular, if the linewidths are inhomogeneous). However, no differences were observed, for any given sample composition, between individually prepared samples or upon heating/cooling. The stability supports the assumption of true equilibrium, and the comparability of intensities for $N = 4, \ldots, 0$ tetrahedra suggests that it is an equilibrium at rather small difference in formation enthalpies for $N = 4, \ldots, 0$ tetrahedra. This is then quantified by the statistical hypothesis underlying figure 10, for the composition $GeSBr_2$.

Upon addition of S, the situation changes. Figure 3 shows strong lines at 150, 210 and 480 cm^{-1}, which are characteristic for S_8 rings. In the same spectra, the $N = 2$ and $N = 3$ group intensities decrease markedly, relative to $N = 4$ and $N = 3$ groups. Thus a disproportionation in favour of S–S bonds apparently takes place. Addition of S did not lead to an increase in $GeS_{4/2}$ tetrahedra, 340 cm^{-1} line, as might have been expected. It has to be kept in mind that S_8 rings are very strong Raman scatterers, so that the intensity observed may only represent a small fraction of S in S_8 rings.

3.3. Linewidths

The linewidths of the TBD modes are presented in table 1, where for simplicity a Lorentzian lineshape has been used. The widths do contain important information on bond angles and distances, on the surroundings, on energy transfer (and in principle particle transfer) rates and on the glass transition. Before discussing these, it appeared necessary, however, to establish a structure model as the basis of any more detailed discussion. This basis is the subject of the present work.

From table 1 we note that linewidths (i) increase drastically from $GeBr_4$ to $GeS_{4/2}$, and (ii) change, for the $GeS_{2/2}Br_2$ and $GeS_{3/2}Br$ lines (270–320 cm^{-1}), from the $GeSBr_2$, GeS_3Br_2 samples to the $GeS_{3/2}Br$ sample. (iii) We add here that the widths of the TBD lines 268, 304 and 356 cm^{-1} of $GeSBr_2$ increase with T, though with different slopes.

Points (i) and (ii) suggest that connectivity is the main reason for the linewidths observed for $N_{Br} < 4$. The increase is roughly 1 cm^{-1} per S bond, surprisingly less than the width of the $GeBr_4$ A_1 mode (1.6 cm^{-1}). To the extent that line intensities are a measure of connectivity, the temperature independence supports the stability of interconnections of tetrahedra, as was discussed in § 3.2. For the simulations in § 4, a rather narrow and constant width of 2 cm^{-1} has been used throughout.

4. Analysis using model calculations

4.1. Models for GeS_2 glass and related substances

GeS_2 glass has been extensively studied (see e.g. Boolchand *et al* 1986, Lucovsky *et al* 1974a, b, Kawamoto and Kawashima 1982, Tenhover *et al* 1985, and references therein).

Table 1. Approximate decomposition of the spectral region 230–350 cm^{-1} for various Ge–S–Br systems, using sums of Lorentzians for the lines. The positions ν (cm^{-1}) are uncertain to 1 cm^{-1} unless otherwise stated, the half widths at half maximum Γ (cm^{-1}) to about 10%, and the intensities I (10^3) to roughly 10% within each sample. The different samples have been measured under similar, but not identical, conditions (0.3 W; 3 s/channel; 1 cm^{-1} resolution). The lines derive from the breathing mode ν_1 of the tetrahedra, and the corresponding substitutions are identified under 'Ident' (except for the 323–331 cm^{-1} line F_2). $GeBr_4$/Bz is $GeBr_4$ dissolved in benzene 1:50. As to the bottom line for the $GeS_{4/2}$ tetrahedra, note that its TBD mode group occurs at 341 cm^{-1} in GeS_2 glass, and at 386 cm^{-1} for $GeS_{4/2}^{4-}$ in solution (Popovic 1983).

	$GeSBr_2$			GeS_3Br_2			GeS_4Br_3		
Ident.	ν (cm^{-1})	Γ (cm^{-1})	I (kHz)	ν (cm^{-1})	Γ (cm^{-1})	I (kHz)	ν (cm^{-1})	Γ (cm^{-1})	I (kHz)
$GeBr_4$	236	1.4	9.4	235	1.6	17	236	1.7	216
$GeS_{1/2}Br_3$	256	2.9	16	256	2.6	10	256	4.5	99
$GeS_{2/2}Br_2$	267	3.8	0.94	267	4.6	2.0	268	4.7	13
	278	3.8	2.1	278	3.5	1.2	277	4.8	10
	286	4.6	2.2	286	6.1	5.2	287	4.1	8.1
	291	4.3	3.7	291	3.7	5.3	292	2.7	13
$GeS_{3/2}Br$	304	8.1	1.7	303	8.2	2.8	303	7.9	2.0
	313	2.9	0.74	313	3.0	1.2			
$GeBr_4F_2$	324	8.4	1.4	323	7.4	2.7	326	7.9	13
$GeS_{4/2}$	356	6.3	2.3	355	6.2	3.6	370	7.5	2.1
	Ge_2SBr_6			$GeS_{1.5}Br$			$GeBr_4$/Bz		
	ν (cm^{-1})	Γ (cm^{-1})	I (kHz)	ν (cm^{-1})	Γ (cm^{-1})	I (kHz)	ν (cm^{-1})	Γ (cm^{-1})	I (kHz)
$GeBr_4$	235	1.4	9.7	235	2.4	0.97	235	1.8	176
$GeS_{1/2}Br_3$	256	1.7	2.8	255	2.4	2.9			
$GeS_{2/2}Br_2$	268	6.2	0.22	267	2.6	0.87			
	277	6.6	0.33	279	3.9	1.8			
	283	2.3	0.20	287	7.3	3.2			
	291	2.7	1.2						
$GeS_{3/2}Br$	302	5.3	0.15	306	16	2.1			
$GeBr_4F_2$	323	6.6	0.53						
	331	7.2	0.28				330	12	8.4
$GeS_{4/2}$	355	4.5	0.076	350	9.8	6.1			

The Ge-centred tetrahedron is the basic building unit, connection to adjoining tetrahedra being made by one sulphur at a common corner, or two sulphurs at a common edge. Intermediate-range order is then the connectivity of nearest-neighbour (NN) or next-nearest-neighbour (NNN) tetrahedra, their geometrical configuration, and perhaps a correlation in chemical composition. In GeS_2 glass, corner sharing appears to be the dominant case (it is entropically favoured). However, edge sharing, known to occur in crystalline GeS_2 (Kawamoto and Kawashima 1982), has been claimed to occur in GeS_2 glass from the radial distribution function and it takes over when S is replaced by Se (Nemanich *et al* 1983, Tenhover *et al* 1985); edge sharing has also been invoked by Galeener (1982) to explain a satellite line in SiO_2. Here, we shall discuss the influence

of S/Br substitution in neighbouring S-bonded tetrahedra and the structure of such subunits of neighbouring tetrahedra on the Raman spectra, focusing on the TBD modes (about 230–360 cm^{-1}). Therefore, the first group of subunits are bitetrahedra. Among tritetrahedral subunits, rings will be strongly Raman-active.

Some of these subunits are known to exist as free molecules, with all 'surface' bonds saturated by the halogen (here Br), and one might suspect that our average N in $GeS_{4-N/2}Br_N$ may be realised by a combination of these species: from $GeBr_4$, to bitetrahedral $Br_3GeSGeBr_3$, to $Ge_3S_3Br_6$ rings and $(GeS_{3/2}Br)_4$ 'adamantane' (Pohl *et al* 1981). The latter has its strongly Raman-active breathing mode line at 377 cm^{-1} (Krebs 1983), but this line is not present in our spectra. A sample favouring Ge_2SBr_6 has been studied (figure 2), and its spectrum shows, as expected (§ 4.3) mainly the symmetric breathing mode at 256 cm^{-1}. The saturated rings would give no clue to the complicated structure extending from 260 to 320 cm^{-1} (see figure 9(*c*)).

Molecular $GeBr_2$, i.e. $(GeBr_2)_2$, has been invoked to explain the 286 cm^{-1} band by Koudelka *et al* (1987). From our model calculations (§ 4.3) it has to be concluded that such molecules are not present in the $GeSBr_2$ system.

We shall assume here a model based on an essentially random substitution of Br and S in the tetrahedra together with random or sterically biased connectivity between them (granted the occurrence of some true molecular species, $GeBr_4$ and S_8). The reasons are the following:

(i) No set of very few, small molecules can explain the spectra; see above. (If molecules become larger than two or three, at most four, tetrahedra, and one admits various configurations, there is little difference from representing them by a set of group frequencies, which corresponds to the present 'subunit' approach.)

(ii) The $GeS_{4/2}$ peak shifts with composition (342 cm^{-1} in GeS_2, 350 cm^{-1} in the sample with composition $GeS_{3/2}Br$, 356 cm^{-1} in $GeSBr_2$; see table 1), indicating a marked coupling between fully connected $GeS_{4/2}$ tetrahedra and partly saturated tetrahedra. A change of Ge–nearest-neighbour force constant depending on the other bond partners of the Ge atom is observed, for example, if these are CH_3 instead of Br (Imai *et al* 1982), but not for exchange of halogens ($GeBr_4$ versus $GeBr_{4-N}Cl_N$; see § 4.2.2).

(iii) If one succeeds in discussing the influence of intermediate-range order on the Raman spectra at least for some fairly clearly specified cases (as e.g. in the $GeSBr_2$ system), one may proceed to use Raman spectra generally for intermediate-range order analysis in systems composed of heavier atoms.

(iv) Statistical weighting of tetrahedral substituents appears the most logical, least-biased starting point. Steric effects *must* be included in a structure discussion.

4.2. Systematics of breathing mode frequencies

4.2.1. Use of NORCOR *program: structure.* For the analysis of the gross and fine structure of the Raman spectra, we have used the computer program NORCOR, furnished by Christen (1978). This program was applied here to subunits of increasing size and varying constitution. The program does not use symmetry coordinates. This is important in the present context because we want to study the effect of substitutional and conformational changes on the spectrum, changes that almost inevitably change symmetry properties. While we concentrate on the modes deriving from the tetrahedral breathing mode (TBD), calculated frequencies of all modes are presented in some cases. The eigenvector obtained for each eigenmode is used as input for the intensity calculation; see § 4.3. It

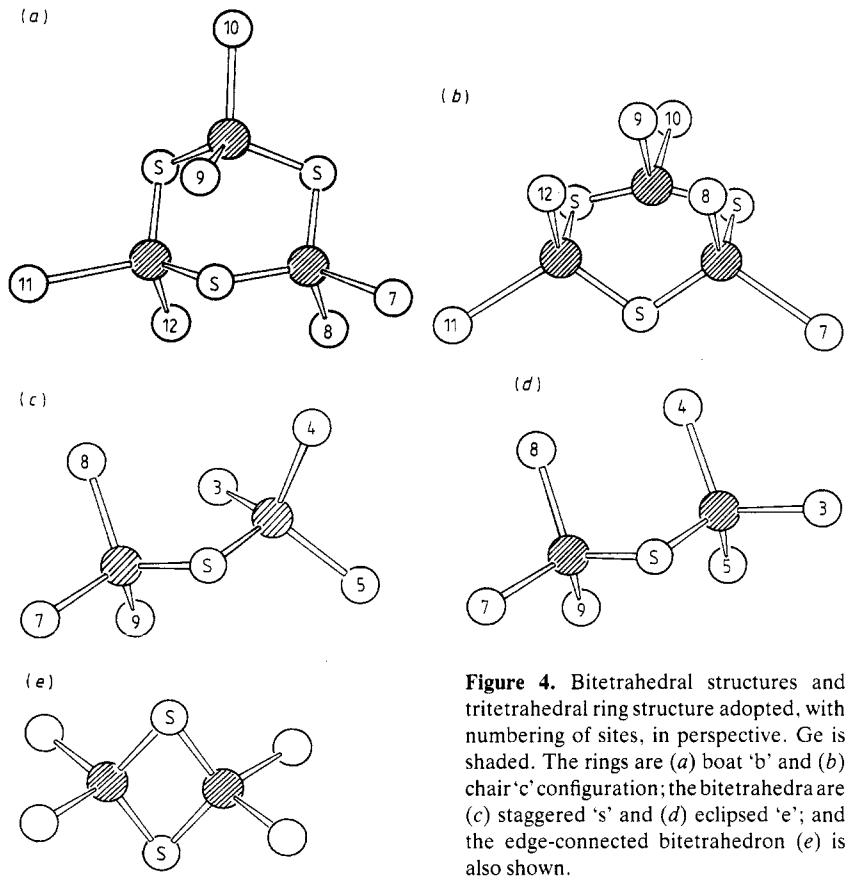

Figure 4. Bitetrahedral structures and tritetrahedral ring structure adopted, with numbering of sites, in perspective. Ge is shaded. The rings are (*a*) boat 'b' and (*b*) chair 'c' configuration; the bitetrahedra are (*c*) staggered 's' and (*d*) eclipsed 'e'; and the edge-connected bitetrahedron (*e*) is also shown.

also allowed us to draw two-dimensional projections of the eigenmode; thus general checks could be made by eye (symmetry, relative size of atomic displacements).

In this analysis, the structure of the tetrahedral units $GeS_{2-N/2}Br_N$ was assumed to be ideal ($\cos\theta_{Ge} = 1/\sqrt{3}$). The 'subunits' or local structures considered are shown in figure 4. Full chemical ordering was assumed in the sense that only Ge–S and Ge–Br bonds were considered, neglecting Ge–Ge, S–S and Br–S bonds. Further details are deferred to § 4.3.4.

One of the great advantages of the Ge–S–Br system is that the standard bond angle at the connecting S, being 105°, leads to a weak coupling of the breathing modes of the tetrahedra, in first approximation a perfect decoupling at 90°. The effect of varying the angle α at the connecting S is displayed for a mixed bitetrahedron in figure 5. In the following we use $\alpha_{GeSGe} = 105°$, keeping in mind that local variations of α_{GeSGe} contribute to line broadening. Because of this decoupling, we have treated outer S atoms of the chosen subunit (i.e. those not bonded to two Ge atoms within that subunit) as if not connected at their second bond. This appears to us a physically justified termination procedure within the network. Addition of a third tetrahedron, say, to a bitetrahedron subunit will effectively broaden the lines.

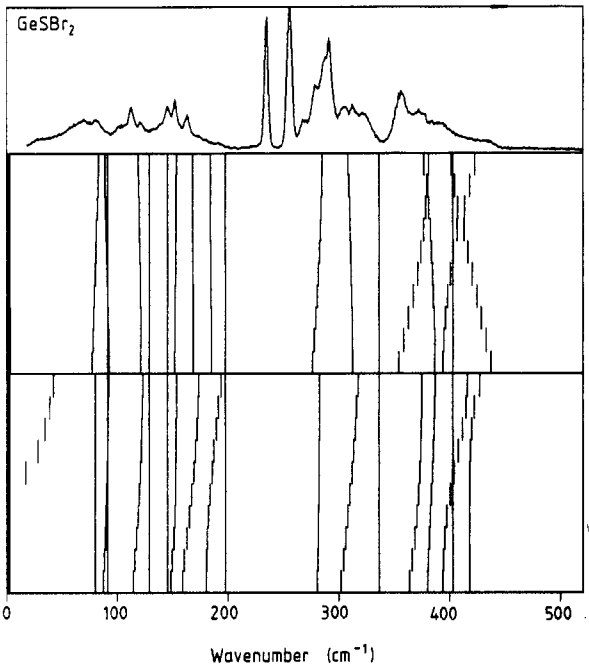

Figure 5. Effect of two parameters that are important for TBD modes on the eigenfrequencies of a bitetrahedral subunit ('e', S: 3, 8, 9, see figure 4): variation of bond angle α_{GeSGe} from 90° (middle) to 120° and variation of $r^2 f_{\alpha(GeSGe)}$ from +0.2 mdyn Å rad^{-2} (bottom) to −0.2 mdyn Å rad^{-2}.

4.2.2. Force constants and geometry. The TBD modes are primarily determined by the radial force constants f_r for Ge–S and Ge–Br and f_{rr} for S–Ge–S, Br–Ge–Br and S–Ge–Br bonds (in the ideal tetrahedron, the force constant of the breathing mode is simply $f_r + 3f_{rr}$). The number of TBD modes is one per tetrahedron in the subunit calculated, and these two or three modes are split by the inter-tetrahedral coupling, effected mainly by f_{rr} and f_α of the Ge–S–Ge bridge(s). For the bond Ge–Br we have made use of the extensive analysis for the Ge halides (pure and mixed) by Cerf (1971). The force constants (mdyn Å^{-1}) are listed in table 2. A short explanation for the values assigned follows:

(i) Wherever the same atomic configuration exists in the Ge halides as in the present systems, force constants f_r, f_{rr}, f_α, etc, were taken from Cerf (1971).

(ii) f_{rr}/f_r was also taken to fulfil the ratio $(f_r - f_{rr})/(f_r + 3f_{rr}) = 0.73$ found by Cerf (1971) for the Ge halides. This is equivalent to the often used assumption $F'/F = -1/10$ in the UBF scheme (Si halides have similar ratios (Höfler 1971)).

(iii) f_r for the Ge–S bond was fitted to the A_1 breathing mode. This leads from the GeS_2 spectrum, $\nu_1 = 342$ cm^{-1}, to $f_r = 1.79$. Since the mode shifts with Br content, we used $f_r = 1.91$ for the $GeSBr_2$ system.

(iv) $r^2 f_\alpha$ for S–Ge–S was set to 0.71 as for Cl–Ge–Cl (Cerf 1971).

(v) For Ge–S–Ge we set $r^2 f_\alpha = 10^{-2}$; this shifts the symmetric, Raman-active TBD mode to the position observed in the Ge_2SBr_6 spectrum, 256 cm^{-1}.

(vi) Force constants involving both Ge–S and Ge–Br, like f_{rr} and f_α for S–Ge–Br, are determined by the rule $f_{AGeB} = (f_{AGeA} f_{BGeB})^{1/2}$.

(vii) Torsion force constants along a Ge–S bond axis were chosen as $+10^{-3}$ if any further S is bonded to the Ge, and as $+10^{-2}$ if a Br is involved because then the 194 cm^{-1} peak in the $Br_3GeSGeBr_3$ system could be reproduced.

Table 2. Force constants used in the simulation for the $GeSBr_2$ system: $f_r, f_{rr}, f_{tor}, f_{ring}$ (mdyn $Å^{-1}$), r^2f_α, $r^2f_{\alpha\alpha'}$ (mdyn Å rad^{-2}) and $rf_{r\alpha'}$ (mdyn rad^{-1}).

$f_{r(GeBr)}$	2.072	(i)			
$f_{r(GeS)}$	1.909	(iii)			
$r^2f_{\alpha(BrGeBr)}$	0.6773	(i)	$r^2f_{\alpha\alpha'(\overset{Br}{Br}Ge\overset{Br}{Br})}$	−0.109	(i)
$r^2f_{\alpha(SGeS)}$	0.71	(iv)	$r^2f_{\alpha\alpha'(\overset{Br}{Br}Ge\overset{S}{Br})}$	−0.12	(x)
$r^2f_{\alpha(BrGeS)}$	0.70	(vi)	$r^2f_{\alpha\alpha'(\overset{S}{Br}Ge\overset{Br}{Br})}$	−0.11	(x)
$f_{rr(BrGeBr)}$	0.176	(i)	$r^2f_{\alpha\alpha'(\overset{Br}{Br}Ge\overset{Br}{S})}$	−0.17	(x)
$f_{rr(SGeS)}$	0.161	(ii)	$r^2f_{\alpha'(\overset{S}{S}Ge\overset{Br}{S})}$	−0.155	(x)
$f_{rr(BrGeS)}$	0.168	(vi)	$r^2f_{\alpha\alpha'(\overset{S}{S}Ge\overset{S}{S})}$	−0.153	(x)
$rf_{r\alpha'(BrGe\overset{Br}{Br})}$	−0.0484	(i)	$r^2f_{\alpha(GeSGe)}$	0.01	(v)
$rf_{r\alpha'(BrGe\overset{Br}{S})}$	−0.059	(x)	$f_{rr(GeSGe)}$	0.161	(x)
$rf_{r\alpha'(BrGe\overset{S}{S})}$	−0.018	(x)	$f_{tor(GeSGeS)}$	0.001	(vii)
$rf_{r\alpha'(SGe\overset{Br}{Br})}$	−0.103	(x)	$f_{tor(GeSGeBr)}$	0.01	(vii)
$rf_{r\alpha'(SGe\overset{Br}{S})}$	−0.023	(x)	$f_{ring((GeS)_3)}$	0.001	(viii)
$rf_{r\alpha'(SGe\overset{S}{S})}$	0.051	(x)	$r^2f_{\alpha\alpha'(ring)}$	0.0	(viii)

For explanation of (i)–(x) see numbered list in § 4.2.2.

(viii) For the ring force constant, $+10^{-3}$ was taken; also $f_{\alpha\alpha'(ring)} = 0$ had to be chosen to avoid unphysical solutions.

(ix) $f_{\alpha\alpha} = 0$ was used from the fit to $GeCl_4$.

(x) Force constants from $GeCl_{4-N}Br_N$ were also transferred to $GeS_{2-N/2}Br_N$ in the cases of $f_{r\alpha'}, f_{\alpha\alpha'}, f_\alpha$ and $f_{rr(GeSGe)}$.

(xi) Since $f_{r\alpha'}$ and $f_{r\alpha}$ appear only in the combination $f_{r\alpha} - f_{r\alpha'}$ as an effective force constant in the calculation of tetrahedral eigenfrequencies (Cerf 1971), $f_{r\alpha}$ was neglected and $f_{r\alpha'}$ set to the effective force constant value.

(xii) The geometrical data were chosen as follows (Å): GeS, $r = 2.014$; GeBr, $r = 2.32$. Angles at Ge in the tetrahedra, 109.4°; and at S in bitetrahedra, 105°; and the same values in the ring $(GeS)_3$.

(xiii) In the edge-connected bitetrahedron, the angle at S was set to 70.6°. All other distances, and the force constants, were unchanged. f_α at S was set to 0.01. For a discussion of edge versus corner-connected $GeS_{4/2}$ tetrahedra, see Popovic (1983) and end of § 4.3.5.

(xiv) The effect of variation of some of the force constants was checked in the same way as that of angle α and force constant $f_{r\alpha}$ at Ge–S–Ge in figure 5; they were found to be much smaller, and are not presented here.

4.2.3. Results. The first result of the calculation of the eigenfrequencies is the well known mass effect of the ligands (here Br, S) on the TBD modes. It is easily recognised from figure 6 where frequency diagrams for all bitetrahedra with unequal number of Br in the two tetrahedra are presented. The effect of eclipsed versus staggered conformation is also presented in figure 6.

Considering only bitetrahedra with unequal substitution, both effects, coupling as well as eclipsed versus staggered conformation, are definitely too small to explain the splitting found within the mass groups $GeS_{2/2}Br_2$ and $GeS_{3/2}Br$.

However, when tetrahedra with the same substitution are coupled ($M = N$), the splitting is markedly larger, up to 20 cm^{-1}, as can be seen from figure 7. Also the

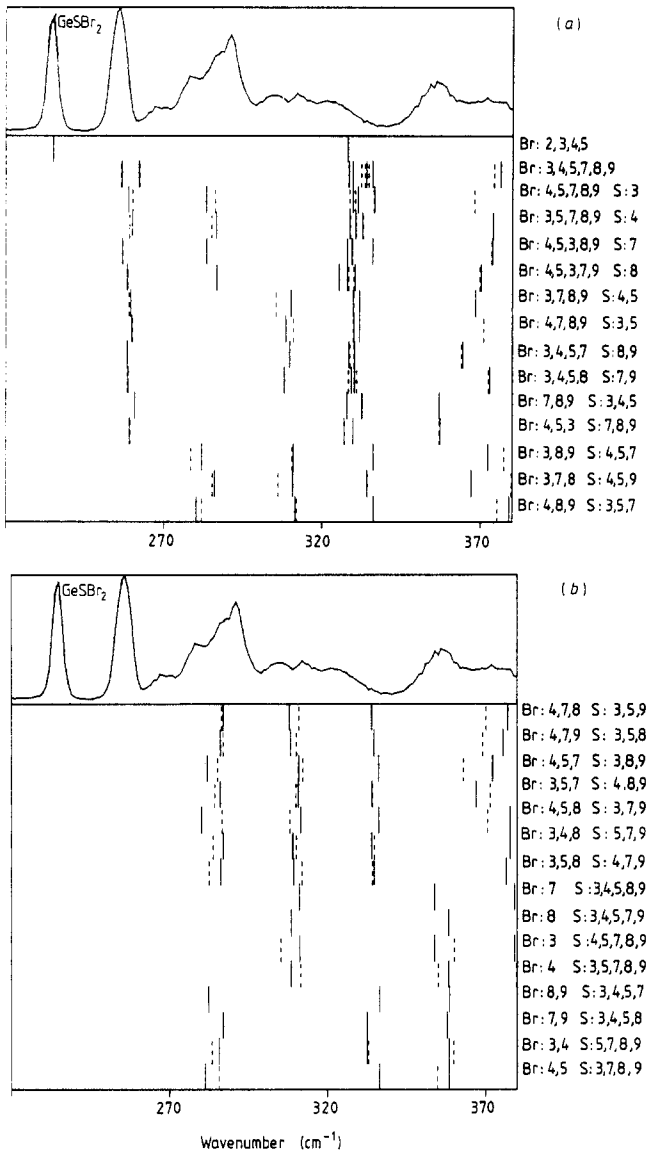

Figure 6. Calculated eigenfrequencies of TBD modes for unequally substituted bitetrahedra ($Br_MS_{3/2-M/2}GeSGeS_{3/2-N/2}Br_N$ with $M \neq N$). On the right-hand side, the sites occupied by Br/S are given, referring to figure 4; the connecting S is always on site 6. Frequencies of eclipsed conformations are full lines, those of staggered conformation are broken lines. The modes beyond 320 cm^{-1} are not TBD modes, except if $M = 0$ or $N = 0$, i.e. S: 3, 4, 5, . . . or S: 7, 8, 9, ... The topmost trace in (*a*) is the $GeBr_4$ tetrahedron.

difference between staggered and eclipsed becomes larger than for $M \neq N$. Both effects are to be ascribed to the near-resonance coupling.

Force constants f_{rr} and f_{α} (at S) also couple neighbouring tetrahedra. Sample calculations on mixed $\{M, N\} = \{3, 2\}$ and equal $\{3, 3\}$ bitetrahedra showed that only very small shifts occur from f_{α} and f_{rr} when these are varied within a reasonable range; see figure 5.

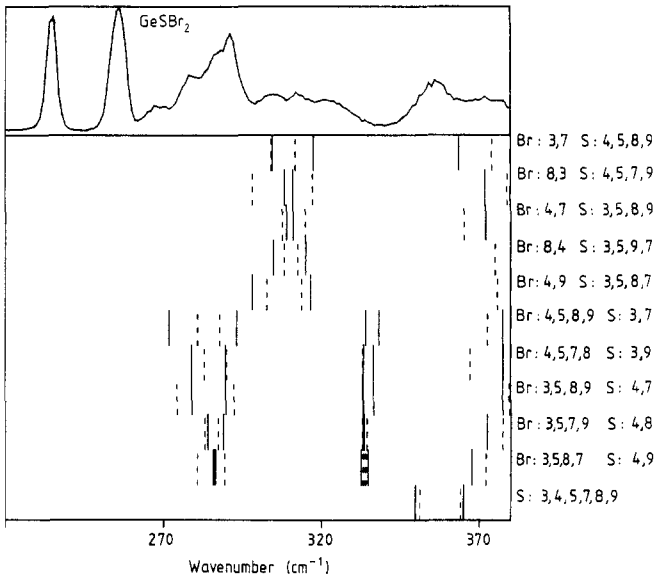

Figure 7. Same as figure 6, but for equally substituted bitetrahedra ($M = N$). In the first five spectra, the tetrahedral F_2 mode (about 340 cm^{-1}) is shifted into the region above 380 cm^{-1}.

If coupling to the neighbours is *not* terminated by halogen cutters, it may become a serious broadening mechanism. This is seen in the $GeS_{3/2}Br$ spectrum of figure 2 where the region 260–310 cm^{-1} is strong (many $GeS_{3/2}Br$ tetrahedra), but constitutes a broad hump very similar to the $GeS_{4/2}$ TBD mode at 340 cm^{-1}.

It is to be remembered that not all the lines in figures 6 and 7 will appear in the observed spectrum, since in most cases one of the TBD modes, viz. the symmetric, lower-frequency mode, is more strongly Raman-active (see § 4.3).

Of the tritetrahedral subunits we have concentrated on the rings since their intensity (relative to three tetrahedral chains) profits most from the coherent breathing motion of the constituent tetrahedra. We present in figure 9 the eigenfrequencies of rings. The $(GeS)_3$ ring can basically be in 'chair' or 'boat' conformation as described in figure 4. We concentrate on the boat conformation for reasons to be discussed in § 4.3.5. The spectra of rings with symmetrical substitution appear in figure 9 ($N_{Br} = \{2,2,2\}, \{1,1,1\}$; for $\{0,0,0\}$ see figure 9(c)).

The similarity of the line positions for different substitutions, seen in table 1, shows that the force constants, effective for the TBD modes, do not change much with the average composition of the sample (except for the $GeS_{4/2}$ tetrahedron).

The frequency of the breathing mode of $GeS_{4/2}$ tetrahedron (ν_1) shifts from 342 cm^{-1} in $GeS_{4/2}$, to 350 cm^{-1} in $GeS_{3/2}Br$, to 356 cm^{-1} in $GeS_{2/2}Br_2$; see table 1.

An improved agreement between calculated and observed mode frequencies (and intensities) could certainly have been achieved by minor adjustments of force constants (an example is the higher F mode at 325 cm^{-1}). At the present stage it seemed more important to pursue a whole analysis *without* adjustments of basic parameters at the various stages of the simulation procedure.

4.3. Spectrum shape simulation

4.3.1. Intensity estimate: procedure. A meaningful comparison between model calculations and experimental spectra is only possible if at least estimates for relative

intensities are included in the calculation. To obtain intensities from *a priori* calculations of electro-optical parameters (see e.g. Reinsch 1985) appears at present hopeless for the systems considered here. Given the eigenvectors of the normal modes, one may base an estimate in a very straightforward manner on atomic polarisabilities as Schrader *et al* (1984) have done or on bond polarisability (Long and Plane 1965). We have chosen the latter *ansatz*, which has been used broadly for the analysis of Raman spectra including heavier atoms (Genzel 1984, Lines 1986, 1987, Barron *et al* 1986), and we follow the procedure used in Montero and del Rio (1976).

The change of the polarisability tensor

$$\boldsymbol{\alpha} = \begin{pmatrix} \alpha & & \\ & \alpha & \\ & & \beta \end{pmatrix}$$

in mode l may be written for a single bond k (i.e. one pair of NN atoms Ge and S or Br):

$$\delta\boldsymbol{\alpha}_k^{(l)} = \{\boldsymbol{\alpha}_\theta, \boldsymbol{\alpha}_\varphi, \boldsymbol{\alpha}_z\}_k \cdot \boldsymbol{u}_k^{(l)}$$
$$\boldsymbol{u}_k^{(l)} = \left(\frac{\delta x_A - \delta x_B}{r}, \frac{\delta y_A - \delta y_B}{r}, \delta z_A - \delta z_B\right)_k^{(l)}. \tag{2}$$

Here x, y, z are coordinates fixed to the bond k, z being along the bond direction; $\boldsymbol{u}_k^{(l)}$ is the maximum change of AB distance vector in normal mode l; $\boldsymbol{u}_k^{(l)} = \boldsymbol{r}_A^{(l)} - \boldsymbol{r}_B^{(l)} - (\boldsymbol{r}_A - \boldsymbol{r}_B)$. Differential changes of $\boldsymbol{\alpha}_k$ upon change of bond length or bond orientation are

$$\boldsymbol{\alpha}_z = \begin{pmatrix} \alpha' & 0 & 0 \\ 0 & \alpha' & 0 \\ 0 & 0 & \beta' \end{pmatrix} \quad \boldsymbol{\alpha}_\theta = \begin{pmatrix} 0 & 0 & 0 \\ 0 & 0 & \beta-\alpha \\ 0 & \beta-\alpha & 0 \end{pmatrix} \quad \boldsymbol{\alpha}_\varphi = \begin{pmatrix} 0 & 0 & \beta-\alpha \\ 0 & 0 & 0 \\ \beta-\alpha & 0 & 0 \end{pmatrix}. \tag{3}$$

We assume rotational symmetry around z. As in Montero and del Rio (1976), after transforming $\delta\boldsymbol{\alpha}_k$ by the rotation $\bar{T}_k$ to a molecule-fixed coordinate system, the contributions $\delta\boldsymbol{\alpha}_k^{(l)}$ of all bonds are added

$$\Delta\boldsymbol{\alpha}^{(l)} = \sum_k \bar{T}_k^{+}\, \delta\boldsymbol{\alpha}_k^{(l)}\, \bar{T}_k. \tag{4}$$

As in the NORCOR program, use of symmetry coordinates would be of little help since most of the subunits considered have very low symmetry. Actually atomic displacement eigenvectors are obtained, within NORCOR, in a chosen molecule-fixed system XYZ; these are first transformed by $\bar{T}_k$ into each bond-fixed system; and then $\Delta\boldsymbol{\alpha}$ is calculated in the molecule-fixed system.

High Raman scattering intensity is expected for TBD modes, and among these the highest intensity is for coherent outward/inward, 'breathing', motion of all bonds in the subunit considered; thus the traceless parts $\boldsymbol{\alpha}_\varphi$, $\boldsymbol{\alpha}_\theta$ will contribute little to the TBD mode scattering. In $\boldsymbol{\alpha}_z$, the element β' is (to our knowledge) usually dominating (see Montero and del Rio 1976). Also, there is an established way of estimating it, based on the work of Long and Plane (1965) if the bond considered has marked covalent contribution as is the case here.

The estimate derives from

$$\beta' = \partial\alpha_{zz}/\partial z \simeq \tfrac{2}{3}(g/Z)(\sigma/a_0)(n/2)z^3. \tag{5}$$

It follows from considering the change in covalent bonding charge when one single bond

Table 3. Electro-optical parameters (10^{-16} cm^2) and refractive index n.

				$GeSBr_2$	
	$GeBr_4$	$GeCl_4$	GeS_2	Ge–S	Ge–Br
α'	1.5[a]	0.95[a]	1.05[b]	1.05[b]	1.5
β'	3.707[c]	2.688[c]	2.906[c]	2.906	3.707
$(\beta - \alpha)/r$	2.0[a]	1.48[a]	2.0[b]	2.0[b]	2.0[b]
n	1.628	1.464		1.82(2)	

[a] From fit to $GeBr_4$ and $GeCl_4$.
[b] Estimated values.
[c] Derived from bond polarisability, equation (5).

is elongated by δz. Here $g/Z = (X_iX_j/Z_iZ_j)^{1/2}$, and X_i (or Z_i) are the electronegativity value (or formal valence) of atom i, $\sigma = \exp(-\Delta X^2/4)$ is the covalent bonding character where $\Delta X = X_A - X_B$; a_0 = Bohr radius; $n/2$ is the number of bonds (here always $n/2 = 1$); and $z = z_A - z_B$ is the equilibrium internuclear distance. The covalent bonding character differs somewhat between Ge–S ($\sigma = 0.95$) and Ge–Br ($\sigma = 0.75$, using the Allred–Rochow scale) which disfavours Br-richer tetrahedra in equation (5).

The electro-optical parameters (EOP) used are presented in table 3. The values β' have been determined from equation (5). Furthermore $\beta - \alpha$ and α' for Ge–Br were determined from a fit to the intensity ratios in $GeBr_4$ (see also § 4.3.2). Other EOP, like finite trace parts of α_θ and α_φ, are neglected. Since we do not strive for absolute intensities, the relation of α with the refractive index appears of no use here.

4.3.2. Intensity estimate: application to specific subunits. Using the eigenvectors obtained from NORCOR, and the EOP listed, the polarised and depolarised Raman intensity I and $I_{VH} = I_{HV}$ were calculated for each mode of each subunit considered as described, e.g. in Montero and del Rio (1976). The resulting calculated intensities (polarised and depolarised) for specific subunits are presented in figures 8 and 9. Figure 8(a) is for one bitetrahedron, and shows the effect of EOP variation; figure 8(b) is the simulation for a $GeCl_4/GeBr_4$ mixture; and figure 9 shows the calculated intensities for various rings.

The TBD modes are mainly determined by the two radial Ge–S and Ge–Br force constants and the two corresponding EOP β'. The influence of substitution and conformation on the TBD mode frequencies and the spectra has been found to be larger than (reasonable) variations of force constants or EOP. This is demonstrated for the EOP in figure 8(a) where spectra for one bitetrahedron are presented, varying β' of the Ge–S bond. It is seen that little change occurs for the TBD modes (i.e. $\partial \ln I_{TBD}/\partial \ln \beta'_{GeS} \simeq 0.6$); the main effect is on the relative intensities of groups of lines at low frequencies (100–200 cm^{-1}) versus TBD modes at high frequencies (400 cm^{-1}), reflecting the basic bending versus symmetric stretching versus asymmetric stretching character of these groups. Reversal of the sign of β_{GeS}/β_{GeBr} was also checked for the bitetrahedron chosen (see figure 8(a)); the reversal has only moderate effect on the absolute intensities of the two TBD modes, and little effect on their relative intensity (but a large effect on the high-frequency modes, which have S and Br motion out of phase). Increasing $(\beta - \alpha)/r = 2.0 \times 10^{-16}$ cm^2 by a factor of 3 does not affect the TBD intensities, while increasing the low-frequency group 100–200 cm^{-1}, as was to be expected.

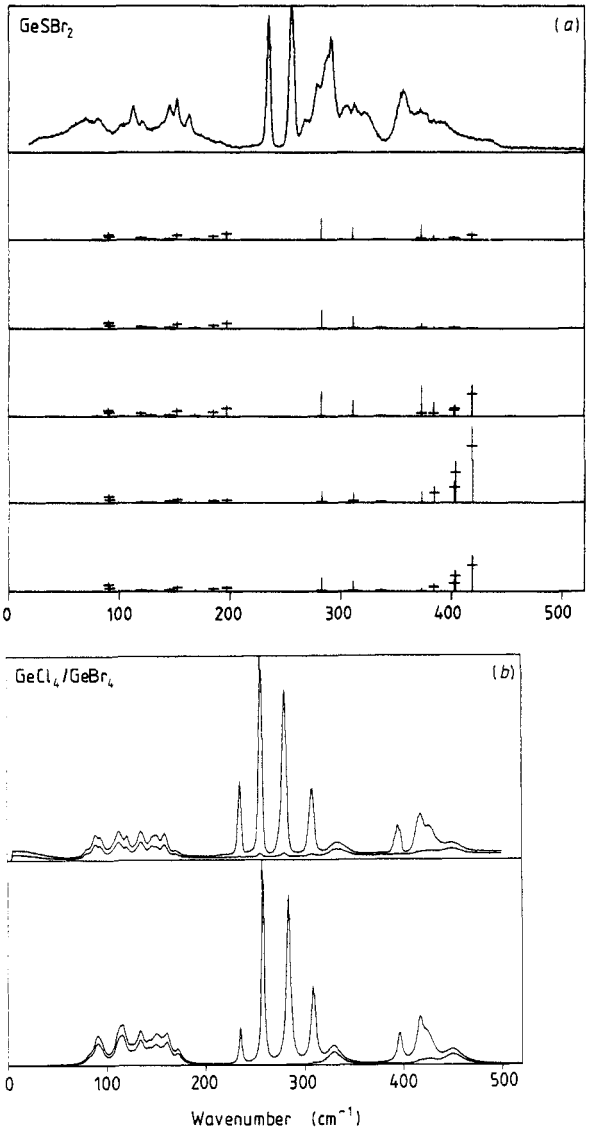

Figure 8. (*a*) Calculated Raman intensities, for one bitetrahedron (Br at positions 4, 5, 7 in figure 4, corner-connected, eclipsed). Polarised intensities (I_{VV}) are presented as vertical bars, depolarised intensities (I_{HV}) are marked by the crossed bars; note that $I_{HV}/I_{VV} \leqslant 0.75$. In the five lower parts the electro-optical parameter β' of equation (5) was changed for the Ge–S bond, while keeping it constant for the Ge–Br bond at $\beta' = 3.7$. From top to bottom: $\beta' = 2.9$ as in all other simulations; $\beta' = 1.46$; 4.4; -2.9; -1.4 respectively. The intensity scale is the same in all parts of this figure, but the scale of (*a*) is 10/12 of figures 9(*a*)–(*c*). (*b*) Calculated Raman intensities for the $GeCl_4/GeBr_4$ mixture, as described in § 4.3.3. The lower part shows this calculation, including linewidths taken from experiment. (For the 0–200 cm^{-1} region they were set to 4 cm^{-1}, for the 330 cm^{-1} group to 7 cm^{-1}, for 418 cm^{-1} to 3.5 cm^{-1}, for 430 cm^{-1} to 5.5 cm^{-1} for 440–500 cm^{-1} to 10 cm^{-1}.) The upper part is the experimental spectrum of the equilibrated 1:1 mixture. VV and HV spectra are presented.

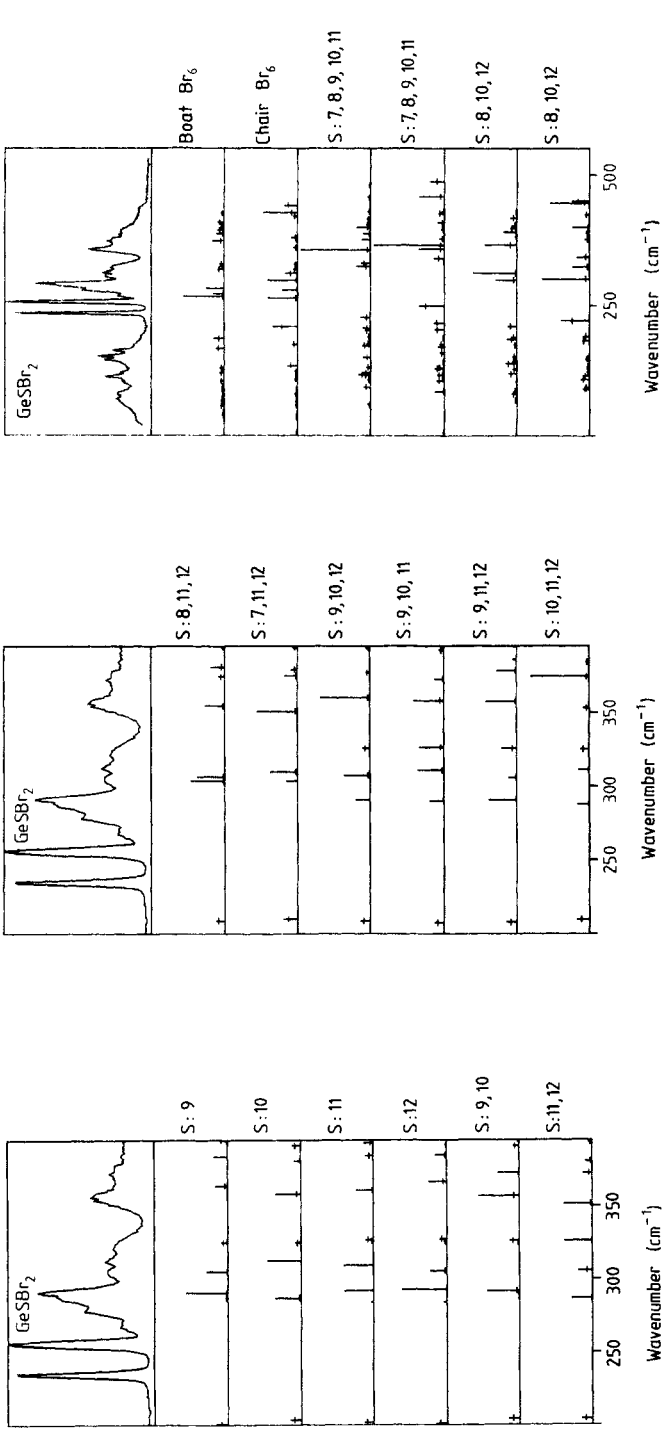

Figure 9. (*a*) Calculated spectra for rings, presented as in figure 8(*a*). Outer sites 7–12 (figure 4) are occupied by Br except for the S sites listed at the right edge of the figure. (*a*) 'Boat' rings with one or two outer S atoms. (*b*) Same as (*a*) for boat rings with three outer S atoms. (*c*) Same as (*a*) for boat and chair rings with three substitutions. From top to bottom: fully brominated $(GeSBr_2)_3$ ring boat, then chair; singly brominated ring boat, then chair; then half brominated ring boat, then chair.

It is this quasi-independence of the calculated intensities of TBD modes, together with the successful simulation of the $GeBr_4/GeCl_4$ system (§ 4.3.3), which allows us to consider the results obtained as reasonably reliable.

For the final spectra we will average over quite a few subunits (§ 4.3.5). Various effects of the surroundings on the individual subunits considered will thus average out (thanks to the central limit theorem and the fact that the neglected perturbations are basically symmetric) leaving the basic effect of β', where we assume that this is really the most important parameter for the TBD modes. Such reasons for perturbations are: continuations of the network; strains and collisions; van der Waals or dipole interaction with non-bonded tetrahedra; accidental resonances; etc.

4.3.3. Simulation for $GeBr_4$–$GeCl_4$ mixture. In order to test the procedure and the parameters as far as possible, we have simulated also the spectrum of a 50:50 mixture of $GeCl_4$ with $GeBr_4$. Force constants for Ge–Cl and Ge–Br as discussed in § 4.2.2 were used in the NORCOR program, with EOP as quoted in table 3. Both sets of parameters had been obtained by reproducing the energies and intensities in pure liquid $GeBr_4$ and $GeCl_4$.

The transfer of force constants and EOP, treated as specific to the individual bond and independent of other bonds in the same tetrahedron, can then be checked by calculating the spectra of the $GeCl_4$–$GeBr_4$ mixture. A statistical substitution in $GeBr_{4-N}Cl_N$ was assumed, i.e. $16p(N) = 1, 4, 6, 4, 1$ for $N = 0, 1, 2, 3, 4$ respectively. The resulting simulation is compared with the experimental spectrum in figure 8(*b*). Here, linewidths have been set close to the experimentally observed widths. We claim that the agreement obtained is very satisfactory (except for the $GeBr_4$ line, which comes out a factor of 2 too weak in the simulation), substantiating the bondwise transferability of parameters. The intensity changes reported in Tenhover *et al* (1985) for $GeSe_{4-N/2}S_{N/2}$ TBD modes seem not to occur in the mixed GeCl/Br tetrahedral molecules. A test of the procedure used here is under way for Ge–S molecular systems.

4.3.4. Line intensity and size of subunits. What is to be treated as a subunit in the present discussion are single tetrahedra and such groups of 2, 3, . . . tetrahedra, within which the tetrahedral breathing modes of the constituent tetrahedra vibrate essentially coherently. The coherence is important because it determines the size of that subunit for which one has to calculate the intensity; schematically

$$I \sim \sum_s p\{s\} \left(\sum_k \alpha \right)_s^2 \tag{6}$$

where s runs over the subunits, $p\{s\}$ is their probability of occurrence (§ 4.3.5), and k runs over the bonds within a coherently vibrating subunit. The size of the subunits to be considered is certainly larger than single tetrahedra (otherwise one misses the fine structure). On the other hand, effects from very distant neighbours will most probably average out in the disordered system: bitetrahedra with different constitution ($N_1 \neq N_2$) are already decoupled energetically, showing only small shifts of the two TBD modes from the two basic (free tetrahedron) A_1 modes; the effect of the coupling on the intensity is seen in figure 8(*a*). Equally substituted tetrahedra on the other hand are relatively rarely direct neighbours: the most important cases are thus $N_1 = 2$, $N_2 = 2$ because of the statistical significance; correspondingly rings of three $N = 2$ tetrahedra. For the rings, the effect of coupling on the intensity is seen in figure 9. In any case, coherent vibration over several tetrahedra will be disturbed by differences in coupling,

non-linearity that leads to interaction with other modes, etc. Thus we expect in a disordered system a decay of coherence of motion already over short distances. We have therefore considered at most three tetrahedra.

In view of this consideration it appears difficult to expect sizable coherent contributions from units as large as 12-atom rings, as were proposed for $GeSe_2$ for example in Phillips (1981), unless these units have an extra stability and thus relatively strong internal coupling, plus an increased occurrence of one configuration (as is the case for S_8).

4.3.5. Choice of subunits, weights and simulations for $GeSBr_2$. Intermediate-range order in a material that is not fully ordered implies necessarily distributions of order parameters. This is expressed here first as the distribution of the Ge tetrahedra over substitution, characterised by $N = 0, \ldots, 4$ in the substitution formula $GeBr_NS_{2-N/2}$. The second, more complicated, distribution is over the connectivity. We consider here bitetrahedra $\{N_1N_2\}$, i.e. subunits consisting of two NN Ge tetrahedra connected by one bridging sulphur, with substitution $N_{Br} = N_1, N_2$ in the two tetrahedra, and with basic geometry eclipsed or staggered; also we consider rings with substitution $\{N_1N_2N_3\}$, and (chair) or (boat) geometry. The intensity contributed by the subunits $\{N\ldots\}, i\{N\ldots\}$, is summed up with a weight factor $p\{N\ldots\}$ to obtain the simulation of the spectrum according to equation (6).

Single tetrahedra. We start from isolated Ge-centred tetrahedra, and assume a statistical, i.e. binomial, distribution for $N_{Br} \equiv N$, with N_{pl} the number of available places, and $\bar{N} = \bar{N}_{Br}$ the average number of Br substituents, which is given by the gross composition

$$p(N) = \binom{N_{pl}}{N}\left(\frac{\bar{N}}{N_{pl}}\right)^N\left(1 - \frac{\bar{N}}{N_{pl}}\right)^{N_{pl}-N}. \tag{7}$$

For the single tetrahedron, $N_{pl} = 4$, and for the average composition $GeSBr_2$, $\bar{N}/N_{pl} = 0.5$, so that the probabilities $p(0), \ldots, p(4)$ are $(1, 4, 6, 4, 1)/16$. The statistical counting implies (i) that only Ge–S and Ge–Br bonding need be considered, (ii) that Ge–S and Ge–Br bonds are energetically close and (iii) that each Ge–S and Ge–Br bonding probability is independent of the other bonds. Assumption (i) is supported by the absence of the S_8 ring lines (they appear only in S-rich samples), and by the weak Br–Br or S–Br bonding energies; moreover chemical ordering, i.e. preference for unequal nearest neighbours, is a general phenomenon in chalcogenide glasses. Assumption (iii) is the obvious first approximation: also a statistical assumption is the least-biased reference. As to (ii), neglect of the energy considerations is suggested for the present systems by the fact that the samples have been prepared at high temperature, and that they show no spectral changes upon heating or cooling cycles.

Among the single $GeS_{2-N/2}Br_N$ tetrahedra, $1/16 = 6.3\%$ are fully saturated, true molecular species $GeBr_4$ in the $GeSBr_2$ sample. As to the remaining 93.7%, we now determine the probability for each substitution $N_{Br} = 0, 1, 2, 3$ to supply its scattering intensity to the total spectrum while it oscillates coherently within a bitetrahedron or a ring (for short, while it forms a bitetrahedron or a ring). The procedure can be sketched as follows (see Sukmanowski 1989).

Bitetrahedra. In the bitetrahedra we assume again statistical substitution Br/S; therefore in the $GeSBr_2$ sample the probability of finding a bitetrahedron with $N_{Br} =$

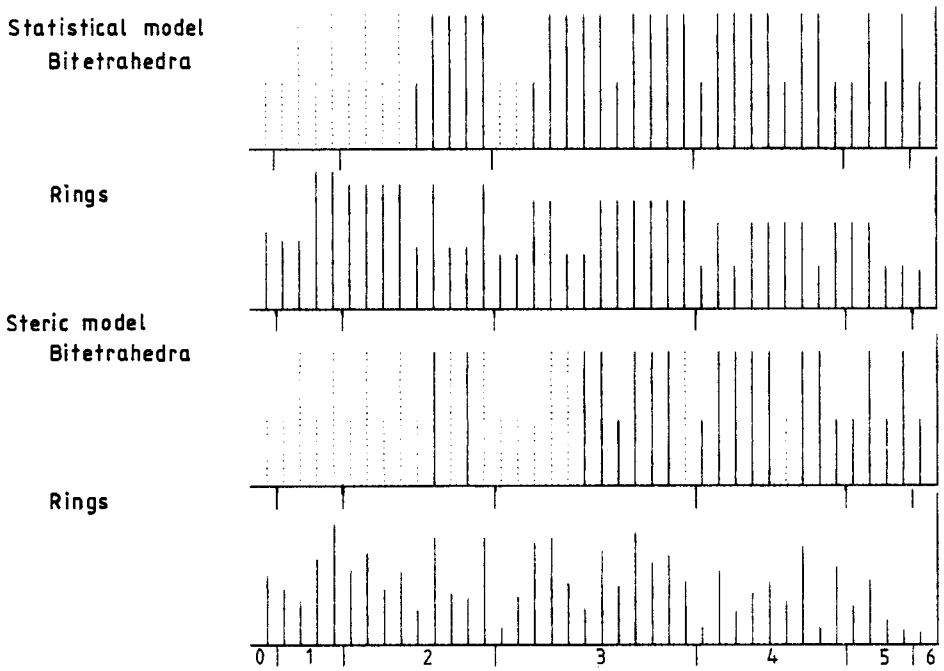

Figure 10. Relative probabilities of the subunits as used for the simulation. Each substitution in a ring or bitetrahedron has a vertical bar, the length of which is its statistical weight. The number of outer S atoms is given underneath. Top band: bitetrahedra (a double length means that this bitetrahedron has a symmetry degeneracy); full (dotted) bars are for bitetrahedra that can (cannot) form rings depending on S content. Second band: rings as derived from statistical model, see § 4.3.5. Third band: bitetrahedra again; full (dotted) bars are for bitetrahedra that can (cannot) form rings, depending on steric reasons and S content. Lowest band: rings as found from the steric model.

$N_1 + N_2 = 0, 1, \ldots, 6$ is respectively $(1.4, 8.8, 22.0, 29.3, 22.0, 8.8, 1.4) \times 10^{-2}$. Note that the last 1.4% are true, saturated molecules $Br_3GeSGeBr_3$. The group of bitetrahedra $\{N_1N_2\}$ comprises a total number of 39 discernible configurations (eclipsed), characterised by the site occupancies (see figure 4) that are given at the side of figures 6 and 7. For each bitetrahedron, the Raman spectrum $i(\nu)$ was calculated as described above; these spectra are not shown for lack of space; for an example, see figure 8(a). In view of the final normalisation among single-, bi- and tritetrahedral subunits, we normalise $i(\nu)$ to the number of tetrahedra (i.e. here by a factor 1/2).

Each discernible configuration is characterised by N_1, N_2, eclipsed (e) or staggered (s), and by the conformation (i.e. by the distribution of the Br atoms over the available sites). Each one has the same weight $p\{N_1N_2, \text{e/s}, \text{conf}\}$, while some of the frequencies will be identical for symmetry reasons. The weights are shown for the 40 possible eclipsed bitetrahedra in figure 10 (first and third rows); from left to right, the number of S atoms increases.

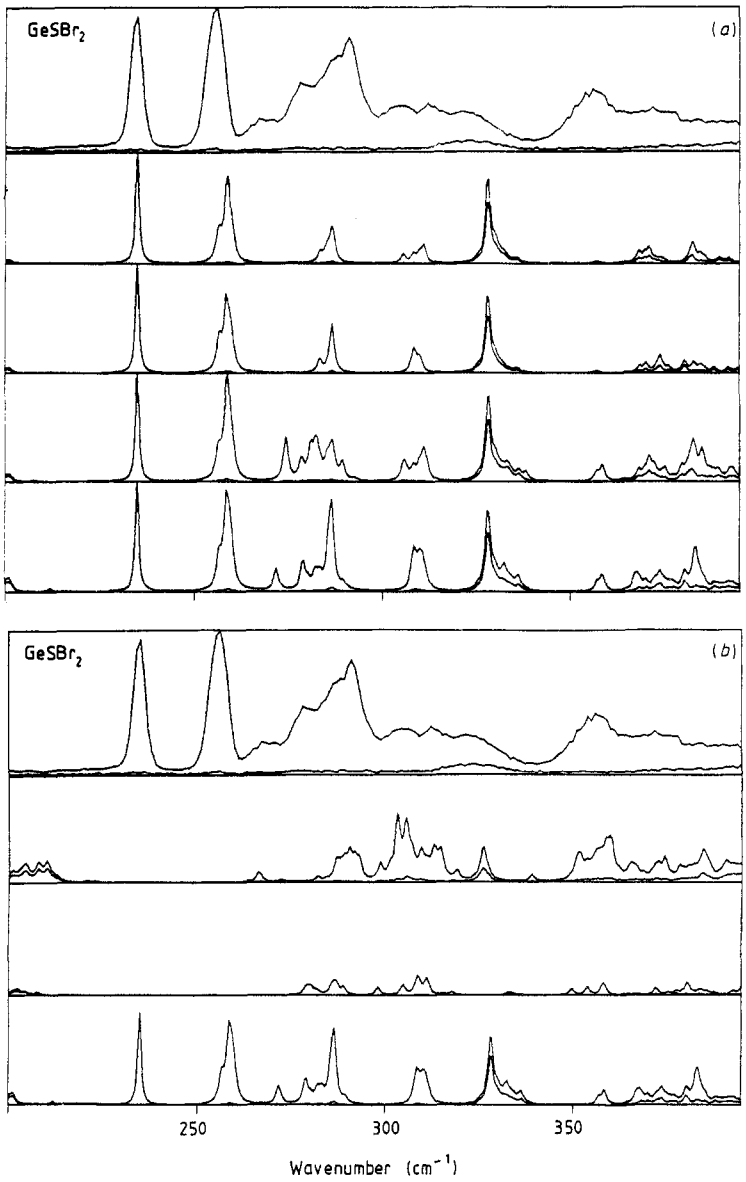

Figure 11. (*a*) Simulations of the Raman spectrum of a $GeSBr_2$ system comprising as subunits only such eclipsed bitetrahedra that cannot be part of a ring (for lack of S or steric reasons). Top band: experimental spectrum; then down to the bottom: model 1 (pure statistics) staggered; model 1 eclipsed; model 2 (steric) staggered; model 2 eclipsed. (*b*) Simulation as in (*a*) for the steric model. Second from top: rings in boat configuration; then down: eclipsed bitetrahedra that can form rings; eclipsed bitetrahedra that cannot form rings.

If one considers no larger subunits, one obtains as the best simulated spectrum the sum of the two lower traces in figure 11(*b*). It is seen that the 'flag' appearance of the $N_{Br} = 2$ group is already found (270–290 cm^{-1}). That the eclipsed configuration appears

to be the best is in accord with the observation that an averaging of the orientations between eclipsed and staggered tends to come close to the spectrum of the eclipsed configuration (Eysel, private communication). However, the characteristic splitting of the $N_{Br} = 1$ group (into 303 and 313 cm^{-1}, table 1) is *not* reproduced. We conclude that one has to consider larger subunits.

Before doing so we turn to a special set of bitetrahedral units, namely those sharing edges, i.e. with two bridging S atoms. Nemanich *et al* (1983) have ascribed the satellite structure at 10% beyond the A mode in $GeSe_2$ to the breathing mode of the $(=GeSe)_2$ ring of edge-sharing tetrahedra (4 atoms). Also, Tenhover *et al* (1985) have based their interpretation of the Raman spectra of $Si(S, Se)_2$ largely on chains of doubly connected tetrahedra, a pattern known to exist in the respective crystalline phases (Kawamoto and Kawashima 1982, Krebs 1983). Now, for this configuration our model calculations predict a high-frequency mode (420–450 cm^{-1}) with high intensity compared to the TBD mode(s) as shown in figure 13 (bottom trace). In the observed spectra, however, no strong line or group is apparent at these frequencies. We conclude that edge sharing may be neglected in the present discussion. The absence is not surprising in view of ample ability of stress-free saturation of bonds, offered in the Ge–S–Br systems considered here.

Tritetrahedra. Returning now to larger subunits, imagine three tetrahedra in a chain. There is a large number of equivalent conformations for each $\{N_1N_2N_3\}$, and no strong intra-subunit coupling compared to the external perturbations. It is therefore very probable that such a tritetrahedral chain cannot vibrate coherently, as an isolated subunit, and therefore the intensity will be assumed to appear in the bitetrahedral spectra. The existence of tritetrahedral chains, etc, and their coupling to further tetrahedra, shows up only in the linewidth of the bitetrahedral spectrum. Subunits consisting of more than three tetrahedra, like a four-tetrahedra star or crown (adamantane-like; Krebs 1983) have rapidly decreasing chance of (i) being composed of equally substituted tetrahedra where the splittings would be large and (ii) being coherently coupled. Their scattering intensity will appear as if caused by independent bi- and/or tritetrahedra. The adamantane-like saturated $Ge_4S_6Br_4$ molecule has its strong Raman line at 363 cm^{-1} (Pohl *et al* 1981), possibly a faint peak in figures 1 and 2.

The subunit 'ring' of three tetrahedra, on the other hand, can be expected to contribute rather specifically to the Raman spectrum, and, as we shall show, inclusion of these subunits allows a very satisfactory simulation of the experimental spectra. Intra-subunit coupling increases the chance for coherent vibration, and has prominent Raman-active modes. The spectra of all rings (which are characterised by $\{N_1N_2N_3\}$ and the site occupancy; figure 4) were calculated for boat or chair configurations of the six-atom ring. Figures 9(*a*) and (*b*) present examples from the calculated intensities in the TDB mode range. Figure 9(*c*) compares 'chair' and 'boat' conformations for two substitutions.

What are the probabilities to be ascribed to each of the rings? We have chosen two approaches, a 'steric' and a 'statistical' approach. The statistical approach is rather simple. Each of the three 'sites' in a ring is occupied independently of the other sites; the possible tetrahedra with $N_S = 2, 3, 4$ take these sites according to their statistical weight (6:4:1). A set of 39 rings is thus produced. The resulting probability distribution is presented in figure 10 (second trace); it is ordered according to the number of sulphur atoms as the 'outside' substitutes, $N_S = 0, \ldots, 6$.

Finally one has to take into account that not all the bitetrahedra, which can form rings, show up as rings in the spectrum (i.e. some rings are perturbed so strongly that

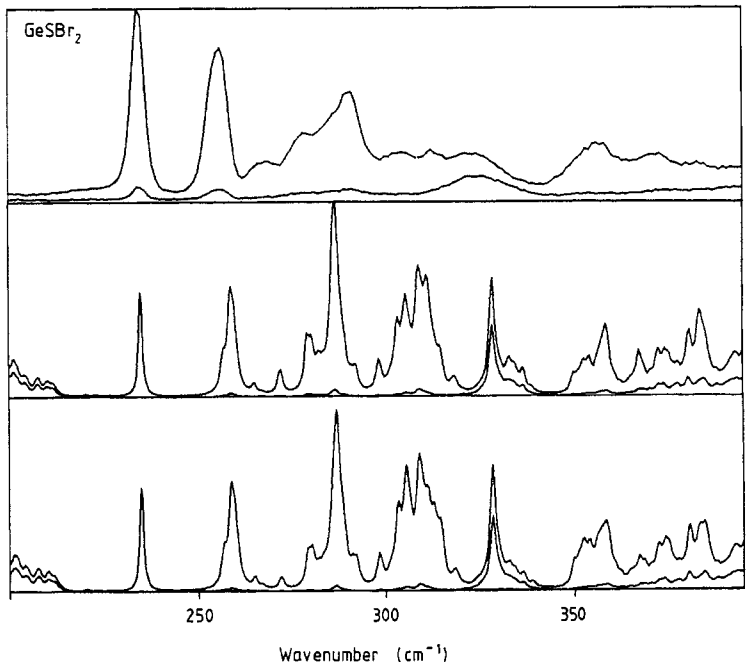

Figure 12. Final results of the simulations for the $GeSBr_2$ system as described in § 4.3. The subunits included are those eclipsed bitetrahedra that cannot form rings, those that can (but do not), and boat rings. Bottom band: statistical model; middle band: steric model; top band: experiment.

the spectrum is approximated better by considering as a coherently vibrating subunit only two adjacent bitetrahedra, whence we are back to the bitetrahedra). We assume for simplicity and unambiguity that this reduces the total spectrum, compared to that from all rings, by a certain fraction, to be taken from experiment. This fraction turns out to be about 0.6; this factor is already included in figure 11(*b*). The result is then the simulation presented in figure 12 (bottom trace).

Now we turn to the 'steric' scheme for the rings. Here we start from each bitetrahedron $\{N_1N_2$, e/c, conf$\}$ and ask whether, in this given fixed configuration, it can be completed to a ring by adding a third tetrahedron; if this is sterically impossible, the bitetrahedron 'cannot form rings', and it is left among the bitetrahedra. If it can form a ring, we count the resulting configuration as ring(s) with relative weight(s) according to that of the bitetrahedron times that of the (various) third tetrahedron(s). Figure 10 presents the relative weights of the rings, in the bottom trace, and above it the weights of the bitetrahedra. Again, not all the rings that are sterically possible will vibrate coherently and a gross reduction factor of 0.6 will be applied; again each ring spectrum is normalised by 1/3.

The simulation using the steric scheme is shown in figure 11(*b*). It is seen that now a prominent group at about 305 cm^{-1} builds up as a signature of the rings. In these simulations, the chair configuration for the rings had been followed on an equal footing with the boats, just as for eclipsed and staggered bitetrahedra. The final simulated spectrum of the group of rings in chair configuration is presented in figure 13 (second

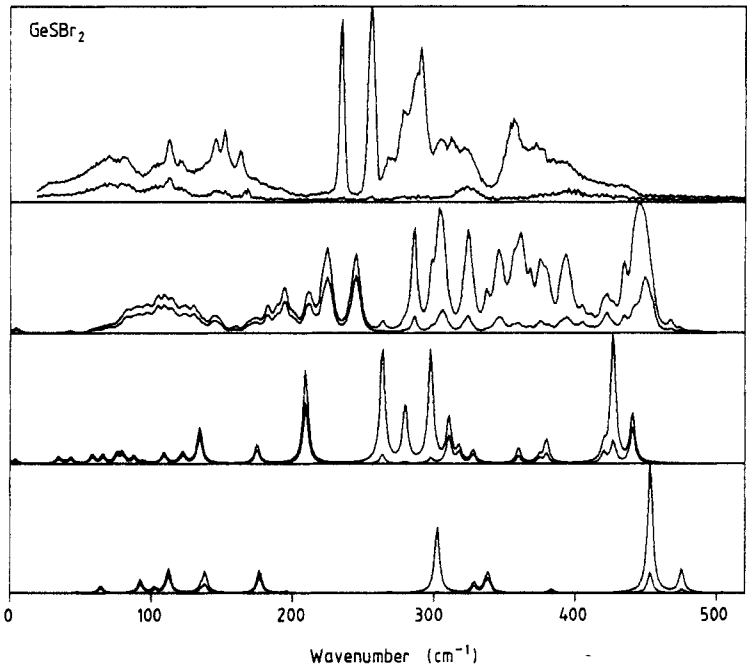

Figure 13. Simulations for configurations that apparently do not contribute noticeably in the $GeSBr_2$ system. Second from top: all rings in chair configuration; next: ring $(GeSBr_2)_3$ in chair configuration; bottom: edge-connected bitetrahedron $(GeS_2)_2$.

trace). It is seen to differ quite a lot from the experiment (figure 13, top), especially at high frequencies (400–450 cm^{-1}), but also around 200 cm^{-1}. This was already indicated by the individual boat and chair spectra in figure 9(*c*). We conclude that the rings in chair configuration are essentially absent in our system $GeSBr_2$.

Final simulations. When both bitetrahedra and boat rings are included in the simulation, we obtain finally the spectra in figure 12 (middle part, steric model; lower part, statistical model for the rings).

4.3.6. Results. The results of the spectrum simulations, based on our model calculations for frequencies and intensities, will now be surveyed. The presentation is based on the concept used here, viz. subunits of increasing size and complexity. The best simulation for $GeSBr_2$ is presented in figure 12 (middle trace).

True molecular units $GeBr_4$ are present in samples of gross composition $GeSBr_2$, $GeS_{3/2}Br$, GeS_3Br_2 and Ge_2SBr_6. Their occurrence in $GeSBr_2$ appears to be about 10%, somewhat stronger than the statistically expected 6.25%. The excess intensity in the (fully symmetric, rather well isolated) $GeBr_4$ line may, however, be an indication for the need to improve the simple model used here for the intensity calculation.

The reasonably isolated lines in the Ge_2SBr_6 sample suggest the presence of true bitetrahedral molecular units $(Br_3Ge)_2S$.

Eclipsed bitetrahedral subunits $Br_{N_1}S_{3/2-N_1/2}GeSGeS_{3/2-N_2/2}Br_{N_2} = \{N_1N_2\}$, which cannot form rings, do produce the characteristic shape (flag structure) in the

region 270–290 cm^{-1}; see figure 11(*a*) (bottom). The flag structure occurs in the $GeSBr_2$, GeS_3Br_2 and Ge_2SBr_6 samples.

Tritetrahedral boat rings $\{N_1N_2N_3\}$, together with the above, appear to reproduce the characteristic shape (double hump) in the region 300–320 cm^{-1}; see figure 11(*b*) (second trace). This double hump is observed in $GeSBr_2$, GeS_3Br_2 and perhaps in $GeS_{3/2}Br$.

The occurrence of the rings has to be reduced to about 60% of the statistical expectation, for a good simulation.

The steric criterion appears to be somewhat favoured over the statistical criterion (§ 4.3.5) for building up rings from bitetrahedra; see figure 12.

Bitetrahedra, edge-connected, $Br_2GeS_2GeBr_2$ as well as tritetrahedral rings in chair configuration seem not to occur; this we conclude from the absence of any strong mode at about 450 cm^{-1}; see figure 13.

Formation of S_8 occurs in S-rich samples GeS_3Br_2; see figure 3.

Electro-optical parameters $\partial\alpha_{zz}/\partial z$ of Ge–S and of Ge–Br bonds have the same sign and comparable magnitude; see § 4.3.2.

5. Conclusions

Raman spectra of halogen-substituted derivatives of the GeS_2 glass forming system have been measured. The halogen (here Br) induces a gross splitting of the breathing mode of the Ge-centred tetrahedra, according to the total mass in the nearest-neighbour shell of Ge. This and similar shifts had been studied earlier in GeS_2-type glasses (Koudelka *et al* 1987, Tenhover *et al* 1985), and they are basically understood as the mass effect (Cervinka 1987). Within this gross structure, a fine structure has been found that is essentially the same for systems with various compositions $GeS_{2-x}Br_{2x}$ and independent of temperature. Its occurrence is due to a favourable interplay of line narrowing (by cutting the network and by the weakness of the coupling of tetrahedra through the connecting S atom), line splitting (by mass and tetrahedron–tetrahedron interaction) and chemical stability of the system. The fine structure can be assigned—we think, conclusively—to the coupling between neighbouring tetrahedra, connected by one S bridge as described in § 4.2, i.e. to intermediate-range order. Intermediate-range order is here formulated and, in principle, fully taken into account by specifying (i) bitetrahedra that occur in various geometrical configurations and chemical substitutions and (ii) sets of three tetrahedra closed to a $(GeS)_3$ ring, again with varying substitution and two structures. We have argued that other subunits (chains of three, four or more, stars of four, and adamantane-like subunits of four tetrahedra, etc) will be found within the broadened lines of these two classes of units, unresolvable at present. The eigen-frequencies and -modes were calculated using a computer program (Christen 1978), which does not employ symmetry. Most force constants and geometrical specifications could be taken over from related molecular Raman spectra; the influence of some further parameters was shown to be not detrimental for an effort to simulate the Raman spectra, since we concentrate on that part of the spectrum derived from the tetrahedral breathing mode. Also the electro-optical parameters of the Ge–S and Ge–Br bonds, which we approximate by their values from the bond polarisability theory, were not critical here. From the calculated simulation, it appears that some geometrical configurations have probabilities markedly below their statistical expectation in the samples studied, namely edge-connected tetrahedra, chair conformed rings, and staggered bitetrahedra. All the

conclusions are based on the good overall simulation of the experimental spectra that has been achieved. For rather complex systems this appears to be the best criterion at present. Thus it seems that an analysis of intermediate-range order in network glass formers is, in favourable systems, within the current possibilities.

Acknowledgments

We are obliged to D Christen for the NORCOR program used. Suggestions from H Eysel and R Steudel are gratefully acknowledged. One of us (IP) worked within the Exchange Program of the Scientific Cooperation between Leningrad University and Free University Berlin. This work is supported by DFG through Sfb 337.

References

Arai K 1983 *J. Non-Cryst. Solids* **59/60** 1059
Barron L D, Escribano J R and Torrance J F 1986 *Mol. Phys.* **57** 653
Bengtzelius U, Götze W and Sjölander A 1984 *J. Phys. C: Solid State Phys.* **17** 5915
Boolchand W, Grothaus J, Tenhover M, Hazle M A and Grasselli R K 1986 *Phys. Rev.* B **33** 5421
Bosse J and Thakur J S 1988 *ILL Workshop on Dynamics of Disordered Materials, Sept.*
Cerf C 1971 *Bull. Soc. Chim.* 2889
Cervinka L 1987 *J. Non-Cryst. Solids* **97/98** 207–12
Christen D 1978 *J. Mol. Struct.* **48** 101–6
Drahokoupil J, Smothlacha O, Fendrych F, Klokocnikova H and Kozlov M A 1986 *J. Non-Cryst. Solids* **88** 43–54
Elliott S R 1987a *J. Non-Cryst. Solids* **97/98** 159
—— 1987b *Phys. Rev. Lett.* **59** 908
Galeener F L 1982 *Solid State Commun.* **44** 103
Genzel L 1984 *Handbuch der Physik* ed. S Flügge, Bd XXV/2d, Sec. 15–19 (Berlin: Springer)
Höfler F 1971 *Z. Naturf.* **26a** 547
Imai Y, Aida K, Sohma K and Watari F 1982 *Polyhedron* **1** 397
Kawamoto Y and Kawashima C 1982 *Mater. Res. Bull.* **17** 1511
Kawamoto Y and Tsuchihashi S 1971 *J. Am. Ceram. Soc.* **54** 131
Koudelka L 1979 *J. Non-Cryst. Solids* **31** 339
Koudelka L, Pisarcik M, Krylov N I and Annaichev V A 1987 *J. Non-Cryst. Solids* **97/98** 1271–4
Krebs B 1983 *Angew. Chem.* **95** 113
Lannin J S 1987 *J. Non-Cryst. Solids* **97/98** 203
Leutheusser E 1984 *Phys. Rev.* A **29** 2765
Lines M E 1986 *J. Chem. Phys.* **60** 1472
—— 1987 *J. Non-Cryst. Solids* **89** 143
Loheider S, Petscherizin I, Soltwisch M, Vögler G and Quitmann D 1990 to be published
Long T V II and Plane R A 1965 *J. Chem. Phys.* **43** 457
Lucovsky G 1987 *J. Non-Cryst. Solids* **97/98** 155
Lucovsky G, deNeufille J P and Galleener F L 1974a *Phys. Rev.* B **9** 1591
Lucovsky G, Galeener F L, Keezer R C, Geils R H and Six H A 1974b *Phys. Rev.* B **10** 5134
Lucovsky G and Martin R M 1972 *J. Non-Cryst. Solids* **8/10** 185
Montero S and del Rio G 1976 *Mol. Phys.* **31** 357–63
Nemanich R J, Galeener F L, Mikkelsen J C Jr, Connell G A N, Etherington G, Wright A C and Sinclair R N 1983 *Physica* B **117/118** 959–61
Phillips J C 1981 *J. Non-Cryst. Solids* **43** 37–77
Pohl S, Seyer U and Krebs B 1981 *Z. Naturf.* **36b** 1432
Popovic Z V 1983 *Phys. Lett.* **94A** 242
Price D L, Susman S and Wright A C 1987 *J. Non-Cryst. Solids* **97/98** 167–70
Reinsch E A 1985 *J. Chem. Phys.* **83** 5784

Rowland S C, Narasimhan S and Bienenstock A 1972 *J. Appl. Phys.* **43** 2741
Schrader B, Spiekermann M, Hecht L and Bongeard D 1984 *J. Mol. Struct.* **113** 49
Soltwisch M, Sukmanowski J and Quitmann D 1987 *J. Chem. Phys.* **86** 3207
Sukmanowski J 1989 *Thesis* Berlin, unpublished
—— 1990 *Int. Symp. Halide Glasses* to appear in *Mater. Sci. Forum*
Tenhover M, Harris J H, Hazle M A, Scher H and Grasselli R K 1985 *J. Non-Cryst. Solids* **69** 249
Thorpe M F and Galeener F L 1980 *J. Non-Cryst. Solids* **35/36** 1197